



# Two-phase flow in high-heat-flux micro-channel heat sink for refrigeration cooling applications: Part I—pressure drop characteristics

Jaeseon Lee, Issam Mudawar \*

*Boiling and Two-Phase Flow Laboratory, School of Mechanical Engineering, Purdue University, West Lafayette, IN 47907 1288, USA*

Received 12 July 2004; received in revised form 10 September 2004

Available online 8 December 2004

## Abstract

Two-phase pressure drop was measured across a micro-channel heat sink that served as an evaporator in a refrigeration cycle. The micro-channels were formed by machining 231  $\mu\text{m}$  wide  $\times$  713  $\mu\text{m}$  deep grooves into the surface of a copper block. Experiments were performed with refrigerant R134a that spanned the following conditions: inlet pressure of  $P_{\text{in}} = 1.44\text{--}6.60$  bar, mass velocity of  $G = 127\text{--}654$   $\text{kg/m}^2\text{s}$ , inlet quality of  $x_{\text{e,in}} = 0.001\text{--}0.25$ , outlet quality of  $x_{\text{e,out}} = 0.49\text{--}$ superheat, and heat flux of  $q'' = 31.6\text{--}93.8$   $\text{W/cm}^2$ . Predictions of the homogeneous equilibrium flow model and prior separated flow models and correlations yielded relatively poor predictions of pressure drop. A new correlation scheme is suggested that incorporates the effect of liquid viscosity and surface tension in the separated flow model's two-phase pressure drop multiplier. This scheme shows excellent agreement with the R134a data as well as previous micro-channel water data. An important practical finding from this study is that the throttling valve in a refrigeration cycle offers significant stiffening to the system, suppressing the large pressure oscillations common to micro-channel heat sinks.

© 2004 Elsevier Ltd. All rights reserved.

*Keywords:* Micro-channels; Flow boiling; Refrigeration; Pressure drop

## 1. Introduction

Two-phase pressure drop has been the subject of extensive research spanning many decades. Starting in the 1940s, researchers were concerned with developing predictive pressure drop models and correlations for mostly traditional industries such as steam and nuclear

power generation, chemical and petroleum, desalination, refrigeration and air conditioning, etc.

With the recent emergence of new applications demanding high-heat-flux dissipation from small areas, the validity of popular pressure drop models and correlations became an open question. These new cooling demands were brought about mostly by the remarkable technological advances in the electronics industry. Since a key measure of improvement in device performance is the ability to integrate the largest number of electronic components in a given surface area, those advances have yielded unprecedented increases in device heat dissipation.

\* Corresponding author. Tel.: +1 765 494 5705; fax: +1 765 494 0539.

E-mail address: [mudawar@ecn.purdue.edu](mailto:mudawar@ecn.purdue.edu) (I. Mudawar).

**Nomenclature**

$A_1, A_2, A_3$	Friedel's correlation constants	$\lambda$	dimensionless number in Lee and Lee correlation
$C$	two-phase multiplier parameter	$\mu$	viscosity
$c_1, c_2, c_3$	correlation constants	$\rho$	density
$C_c$	contraction coefficient	$\sigma$	surface tension
$C_{vt}$	two-phase parameter based on laminar liquid–turbulent vapor flow	$\sigma_c$	contraction area ratio
$C_{vv}$	two-phase parameter based on laminar liquid–laminar vapor flow	$\sigma_e$	expansion area ratio
$d$	diameter	$\phi$	two-phase pressure drop multiplier
$d_h$	hydraulic diameter	$\psi$	dimensionless number in Lee and Lee correlation
$f$	fanning friction factor	$\omega$	volumetric quality
$Fr$	Froude number		
$g$	gravitational acceleration	<i>Superscript</i>	
$G$	mass velocity (kg/m <sup>2</sup> s)	–	two-phase
$h$	enthalpy (J/kg)		
$L$	length	<i>Subscripts</i>	
$P$	pressure (Pa)	a	acceleration
$q''$	heat flux through heat sink base area (W/m <sup>2</sup> or W/cm <sup>2</sup> )	c	critical; contraction
$Re$	Reynolds number based on channel hydraulic diameter	e	expansion
$v$	specific volume (m <sup>3</sup> /kg)	exp	experimental
$We$	Weber number	f	saturated liquid; frictional
$X$	Martinelli parameter	fo	liquid only in entire channel
$x_e$	thermodynamic equilibrium quality	g	saturated vapor
$z$	stream-wise coordinate	in	channel inlet
		out	channel outlet
		pred	predicted
		sp	single phase
		tp	two phase
		tot	total

*Greek symbols*

$\alpha$	void fraction
$\beta$	channel aspect ratio

Cooling of electronic devices is fundamentally different from that of most conventional applications since not only does the heat needs to be removed from the device surface, but the device must also be maintained at a relatively low temperature.

Compounding this problem is the existence of an appreciable thermal resistance between the device and coolant, which is the result of various intermediate layers that are required for electronic packaging and interconnect. To compensate for the ever-increasing heat flux, maintaining an acceptable device temperature therefore requires simultaneously (1) enhancing the convective heat transfer coefficient and (2) reducing the coolant temperature. Those concerns are key drivers behind the recent interest in using refrigerant-cooled micro-channel heat sinks.

A micro-channel heat sink possesses many unique attributes that are ideally suited for electronics cooling. Those include superior cooling characteristics, compactness, and minimal coolant usage, especially when the

coolant changes phase inside the heat sink. Phase change capitalizes upon the coolant's latent heat of vaporization to absorb and ultimately dissipate a larger amount of heat than a single-phase coolant. Furthermore, the heat is removed at a fairly constant temperature that is dictated largely by the coolant's saturation temperature. Unlike single-phase heat sinks that compensate for the large heat removal by incurring an appreciable stream-wise temperature rise in both the coolant and heat sink, phase change maintains better temperature uniformity in the heat sink and aids in preventing local hot spots in the device surface.

However, two-phase micro-channel heat sinks are not without drawbacks. The small hydraulic diameter of a micro-channel can lead to appreciable pressure drop and corresponding increase in power consumption, which is undesirable in electronic systems. Therefore, a strong understanding of the relationship between pressure drop, flow rate and heat flux is of paramount importance to micro-channel heat sink design.

Many of the two-phase pressure drop models and correlations used in industry today stem from the pioneering Lockhart–Martinelli [1] formulation, which has been modified by many investigators in pursuit of better predictions for macro-channels (e.g., Friedel [2], Chisholm [3]). However, recent studies have shown this formulation produces poor predictions when attempted with small channels, suggesting different flow characteristic must be prevalent in the smaller channels.

Bowers and Mudawar [4] were the first to provide a systematic assessment of the unique attributes of pressure drop across micro-channel heat sinks. To examine the influence of hydraulic diameter, they compared the pressure drop for refrigerant R113 in both mini-channel ( $d = 2.54\text{ mm}$ ) and micro-channel ( $d = 510\text{ }\mu\text{m}$ ) heat sinks. Using the homogeneous equilibrium model, they pointed out the serious drawbacks of a very small hydraulic diameter caused by the excessive pressure drop associated with acceleration of the two-phase mixture. Mishima and Hibiki [5] modified the two-phase multiplier in the Lockhart–Martinelli with a new parameter to improve pressure drop prediction for air–water flow in vertical capillary tubes with diameters of  $d = 1\text{--}4\text{ mm}$ . Triplett et al. [6] investigated air–water flow in small circular tubes ( $d = 1.1, 1.45\text{ mm}$ ) and triangular channels ( $d_h = 1.09, 1.49\text{ mm}$ ). The homogeneous equilibrium model showed good predictions for the bubbly and slug flow regimes but not the annular, and the Friedel's correlation (based on the separated flow model) was less accurate than the homogeneous model. Tran et al. [7] investigated two-phase flow of refrigerants R134a, R12, and R113 in small circular channels ( $d = 2.46, 2.92\text{ mm}$ ) and a rectangular channel ( $d_h = 2.40\text{ mm}$ ). Most separated flow models predicted pressure drop values that were smaller than measured. Therefore, they developed a new correlation to better account for the effects of surface tension and channel diameter. Lee and Lee [8] modified the Lockhart–Martinelli two-phase multiplier with a new parameter they correlated from their own data for air–water flow in rectangular channels ( $d_h = 0.784, 6.67\text{ mm}$ ). Zhang and Webb [9] investigated two-phase flow of refrigerants R134a, R22 and R404a in parallel circular channels ( $d = 2.13\text{ mm}$ ) and recommended a new pressure drop correlation based on the separated flow model. Kawahara et al. [10] investigated water–nitrogen flow in a  $100\text{ }\mu\text{m}$  circular tube. They reported the homogeneous flow model generally overpredicted pressure drop data, while the separated flow model using a modified two-phase flow multiplier showed better agreement.

Recently, Qu and Mudawar investigated the fundamental features of two-phase flow and heat transfer in a water-cooled micro-channel heat sink [11,12]. Their work culminated in a comprehensive theoretical model which yielded good predictions of two-phase pressure drop and heat transfer.

The present study is an extension of recent efforts by Mudawar and co-workers to develop a comprehensive method for determining micro-channel heat sink pressure drop for coolants with drastically different thermo-physical properties. New experiments were performed with R134a that were complimented by flow visualization. The heat sink was incorporated as an evaporator in a refrigeration cycle in an effort to achieve the aforementioned goals of high-flux removal while maintaining low surface temperatures. Using both the new R134a pressure drop data as well as Qu and Mudawar's earlier water data, a new correlation scheme is recommended for two-phase pressure drop determination. This scheme is shown to yield far better accuracy than prior macro-channel and small channel correlations. Also discussed in this paper are various unique features of pressure drop in micro-channel evaporators and the suitability refrigerant-cooled heat sinks to electronic cooling applications.

## 2. Experimental methods

### 2.1. Apparatus and measurement techniques

Fig. 1 shows the test facility constructed for this study resembled a conventional refrigeration cycle save for using the micro-channel evaporator. The working fluid used in this study, R134a, is an environmentally friendly non-ozone-depleting HFC refrigerant with overwhelming popularity in most domestic refrigeration and air conditioning applications. Vapor compression was achieved with a DC rotary compressor whose power was determined from its measured current and voltage input. Heat was rejected from the loop via a conventional fin-tube condenser fitted with a cross-flow fan. The fan speed was controlled with a variable voltage transformer that helped modulate the subcooling of the two-phase mixture exiting the condenser. Throttling from high to low pressure was achieved by a manual metering valve situated upstream of the micro-channel evaporator test section.

Fig. 2 shows the primary components of the test section: a transparent polycarbonate cover plate, a G-10 fiberglass housing, an oxygen-free copper micro-channel heat sink, three cartridge heaters, and a G-10 support plate. The micro-channels were formed by cutting 53 of  $231\text{ }\mu\text{m}$  wide and  $713\text{ }\mu\text{m}$  deep micro-slots into the  $25.3\text{ mm} \times 25.3\text{ mm}$  top surface of the copper heat sink. The polycarbonate plastic (Lexan) cover formed the top surface for the micro-channels. The G-10 housing included upstream and downstream plenums to ensure uniform flow distribution between micro-channels and facilitate pressure and temperature measurement both upstream and downstream of the micro-channels. The copper heating block was encased in an insulating

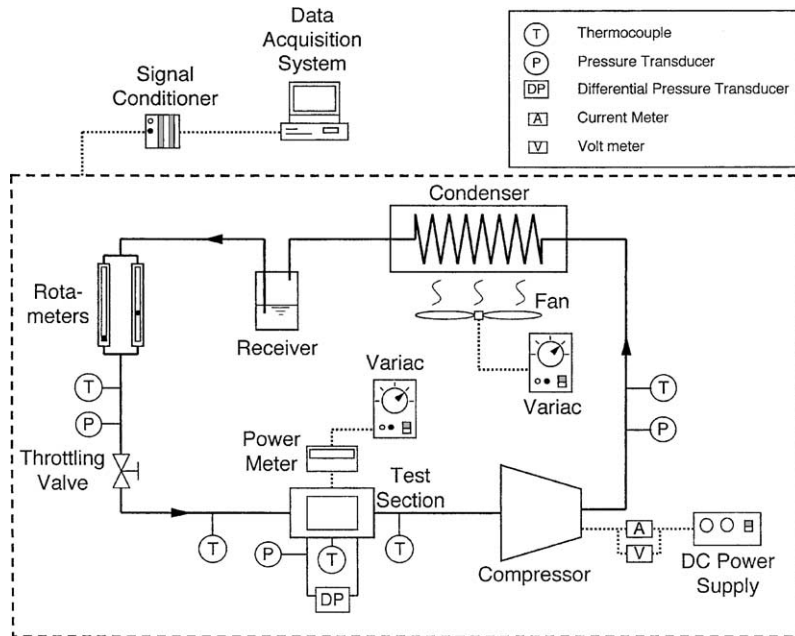


Fig. 1. Schematic of test loop.

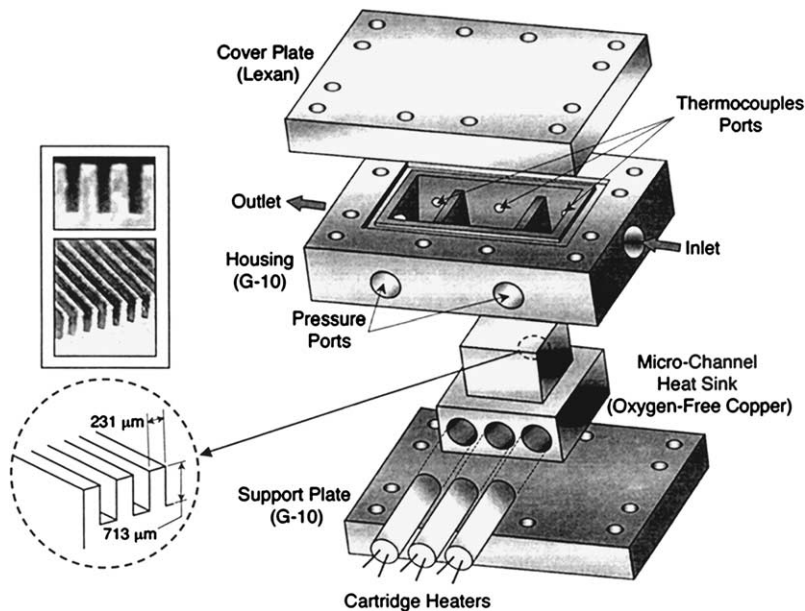


Fig. 2. Construction of micro-channel evaporator test section.

blanket to reduce heat loss to the ambient. Heat was supplied by the cartridge heaters that were embedded beneath the micro-channels; these heaters were powered by a variable voltage transformer.

Two type-T thermocouples were inserted in the inlet and outlet plenums to measure fluid temperature at

those locations. Another type-K thermocouple was inserted in the copper block halfway along the micro-channels. An absolute pressure transducer measured the inlet plenum pressure and a differential pressure transducer the pressure drop between the inlet and outlet plenums. Additional type-T thermocouples and

absolute pressure transducers were located both downstream of the compressor and upstream of the throttling valve. A precision power meter connected to the cartridge heaters' variable voltage transformer was used to measure heat input to the coolant in the evaporator. All thermocouple and pressure transducer measurement signals were transferred to an NI-SCXI signal conditioner interfaced to data acquisition PC. The flow rate of R134a entering the micro-channel evaporator was measured by a glass rotameter situated downstream of the condenser, which also served as a visual indicator of liquid state at that location.

The rotameter provided better than 2% accuracy in flow rate measurement. Errors in the pressure transducer and thermocouple measurements were less than 0.5% and  $\pm 0.3^\circ\text{C}$ , respectively. Heat loss from the heat sink was estimated at less than 4% of the electrical power input.

### 2.1.1. Determination of operating conditions

The refrigerant left the compressor in superheated vapor state and was returned to subcooled liquid after passing through the condenser. Afterwards, the liquid was converted to a two-phase mixture by flashing across the throttling valve. The two-phase mixture entered the evaporator and was converted to superheated vapor before entering the compressor and repeating the cycle.

The mass flow rate of refrigerant entering the evaporator was calculated as the product of volumetric flow rate of liquid measured by the rotameter, and the density of liquid calculated from the temperature and pressure measurements. Since the throttling process is isenthalpic, the evaporator inlet enthalpy was determined from the liquid temperature and pressure measured downstream of the condenser. Using this enthalpy value and the evaporator measured inlet temperature or pressure provided accurate determination of the evaporator's inlet quality,  $x_{e,\text{in}}$ .

Experimental data were acquired over the following range of parameters: inlet pressure of  $P_{\text{in}} = 1.44\text{--}6.60$  bar, mass velocity of  $G = 127\text{--}654$  kg/m<sup>2</sup>s, inlet quality of  $x_{e,\text{in}} = 0.001\text{--}0.25$ , outlet quality of  $x_{e,\text{out}} = 0.49\text{--}1.0$  (superheat), and heat flux of  $q'' = 31.6\text{--}93.8$  W/cm<sup>2</sup>.

## 3. Results and discussion

### 3.1. Pressure drop determination

The evaporator pressure drop measured by the differential pressure transducer includes the sudden contraction loss at the micro-channel inlet and sudden expansion recovery at the outlet. Within the micro-channels, the two-phase pressure drop consists of frictional

and accelerational components. Should the two-phase mixture undergo complete conversion to vapor within the micro-channel, a pressure drop corresponding to pure vapor flow would also be incurred in the downstream region of the micro-channels. In this case, the total pressure drop between the upstream and downstream plenums can be expressed as

$$\Delta P_{\text{tot}} = \Delta P_c + (\Delta P_f + \Delta P_a)_{\text{tp}} + \Delta P_{\text{sp,g}} - \Delta P_e. \quad (1)$$

The contraction pressure loss and expansion recovery were determined from the following relations [2]:

$$\Delta P_c = \frac{G^2 v_f}{2} \left[ \left( \frac{1}{C_c} - 1 \right)^2 + \left( 1 - \frac{1}{\sigma_c^2} \right) \right] \left[ 1 + \frac{v_{\text{fg}} x_{e,\text{in}}}{v_f} \right] \quad (2)$$

and

$$\Delta P_e = G^2 \sigma_c (1 - \sigma_c) v_f \left[ 1 + \frac{v_{\text{fg}} x_{e,\text{out}}}{v_f} \right]. \quad (3)$$

The contraction coefficient  $C_c$  is a function of the contraction ratio  $\sigma_c$  [2]. If the refrigerant exits the micro-channels as pure vapor, the exit quality  $x_{e,\text{out}}$  in the pressure recovery term should be set equal to unity.

When the refrigerant is completely converted into vapor within the micro-channel, the pressure drop for the vapor flow region can be determined from the following relation [13,14]:

$$\Delta P_{\text{sp,g}} = \frac{2L_{\text{sp}}}{d_h} f_{\text{sp,g}} G^2 v_g, \quad (4)$$

where

$$f_{\text{sp,g}} Re_g = 24 [1 - 1.3553\beta + 1.9467\beta^2 - 1.7012\beta^3 + 0.9564\beta^4 - 0.2537\beta^5] \quad \text{for } Re_g < 2000, \quad (5a)$$

$$f_{\text{sp,g}} = 0.079 Re_g^{-0.25} \quad \text{for } 2000 < Re_g < 20,000, \quad (5b)$$

and

$$f_{\text{sp,g}} = 0.046 Re_g^{-0.2} \quad \text{for } 20,000 < Re_g. \quad (5c)$$

The remaining contributions to the evaporator pressure drop are the two-phase frictional and accelerational components. These are discussed in the next section.

### 3.2. Two-phase pressure drop models

#### 3.2.1. Homogeneous equilibrium model (HEM)

The homogeneous equilibrium model is based on the assumption that the two-phase mixture behaves as a pseudo single-phase fluid with mean properties that are weighted relative to vapor and liquid content, and that only latent heat may be exchanged between the phases. Property variations resulting from pressure changes along the micro-channel result in complicating terms that account for kinetic energy changes, flashing, and

compressibility [4]. The resulting pressure gradient may be expressed as

$$Re_{tp} = \frac{Gd_h}{\mu_{tp}} \tag{8}$$

$$-\left(\frac{dP}{dz}\right)_{tp} = \frac{\frac{2f_{tp}}{d_h} G^2 (v_f + x_e v_{fg}) + \frac{4q'' G v_{fg}}{d_h [h_{fg} + G^2 v_{fg} \{x_e v_g + (1 - x_e) v_f\}]}}{1 + G^2 \left\{ x_e \frac{dv_g}{dP} + (1 - x_e) \frac{dv_f}{dP} \right\} \left[ 1 - \frac{G^2 v_{fg} \{x_e v_g + (1 - x_e) v_f\}}{h_{fg} + G^2 v_{fg} \{x_e v_g + (1 - x_e) v_f\}} \right] - \left[ \frac{G^2 v_{fg} \left\{ x_e \frac{dh_g}{dP} + (1 - x_e) \frac{dh_f}{dP} \right\}}{h_{fg} + G^2 v_{fg} \{x_e v_g + (1 - x_e) v_f\}} \right]} \tag{6}$$

The first term in the numerator of Eq. (6) is the frictional gradient and the second the accelerational. The denominator includes kinetic energy, flashing and compressibility terms. The two-phase pressure drop can be determined by integrating Eq. (6) numerically along the stream-wise direction.

$$\Delta P_{tp} = \int_0^{L_{tp}} -\left(\frac{dP}{dz}\right)_{tp} dz \tag{7}$$

A key unknown in the two-phase pressure drop calculation using HEM is the two-phase friction factor,  $f_{tp}$ , which is a function of the two-phase Reynolds number

Table 1 shows the relations used to determine  $f_{tp}$  as well as several popular models of two-phase mixture viscosity,  $\mu_{tp}$ .

Fig. 3 compares pressure drop predictions based on HEM (in addition to  $\Delta P_c$ ,  $\Delta P_{sp,g}$  and  $\Delta P_e$ ) and each of the two-phase viscosity models with the experimental data. The mean absolute error (MAE), defined as

$$MAE = \frac{1}{N} \sum \left[ \frac{|\Delta P_{pred} - \Delta P_{exp}|}{\Delta P_{exp}} \times 100 \right] \tag{9}$$

was used to estimate the accuracy of model predictions. Fig. 3 shows the HEM models yield appreciable

Table 1  
Two-phase mixture viscosity models adopted in the homogenous equilibrium flow model

$$f_{tp} Re_{tp} = 24[1 - 1.3553\beta + 1.9467\beta^2 - 1.7012\beta^3 + 0.9564\beta^4 - 0.2537\beta^5] \quad \text{for } Re_{tp} < 2000$$

$$f_{tp} = 0.079 Re_{tp}^{-0.25} \quad \text{for } 2000 < Re_{tp} < 20,000$$

$$f_{tp} = 0.046 Re_{tp}^{-0.2} \quad \text{for } 20,000 < Re_{tp}$$

Author(s) [Ref.]	Two-phase mixture viscosity model
McAdams [12]	$\frac{1}{\mu_{tp}} = \frac{x_e}{\mu_g} + \frac{(1 - x_e)}{\mu_f}$
Ackers [15]	$\mu_{tp} = \frac{\mu_f}{[(1 - x_e) + x_e (\frac{\mu_f}{\mu_g})^{0.5}]}$
Cicchitti et al. [2]	$\mu_{tp} = x_e \mu_g + (1 - x_e) \mu_f$
Dukler [2]	$\mu_{tp} = \rho_{tp} [x_e v_g \mu_g + (1 - x_e) v_f \mu_f]$
Beattie and Whalley [16]	$\mu_{tp} = \omega \mu_g + (1 - \omega)(1 + 2.5\omega) \mu_f$
	$\omega = \frac{x_e v_g}{v_f + x_e v_{fg}}$
Lin et al. [17]	$\mu_{tp} = \frac{\mu_f \mu_g}{[\mu_g + x_e^{1.4} (\mu_f - \mu_g)]}$

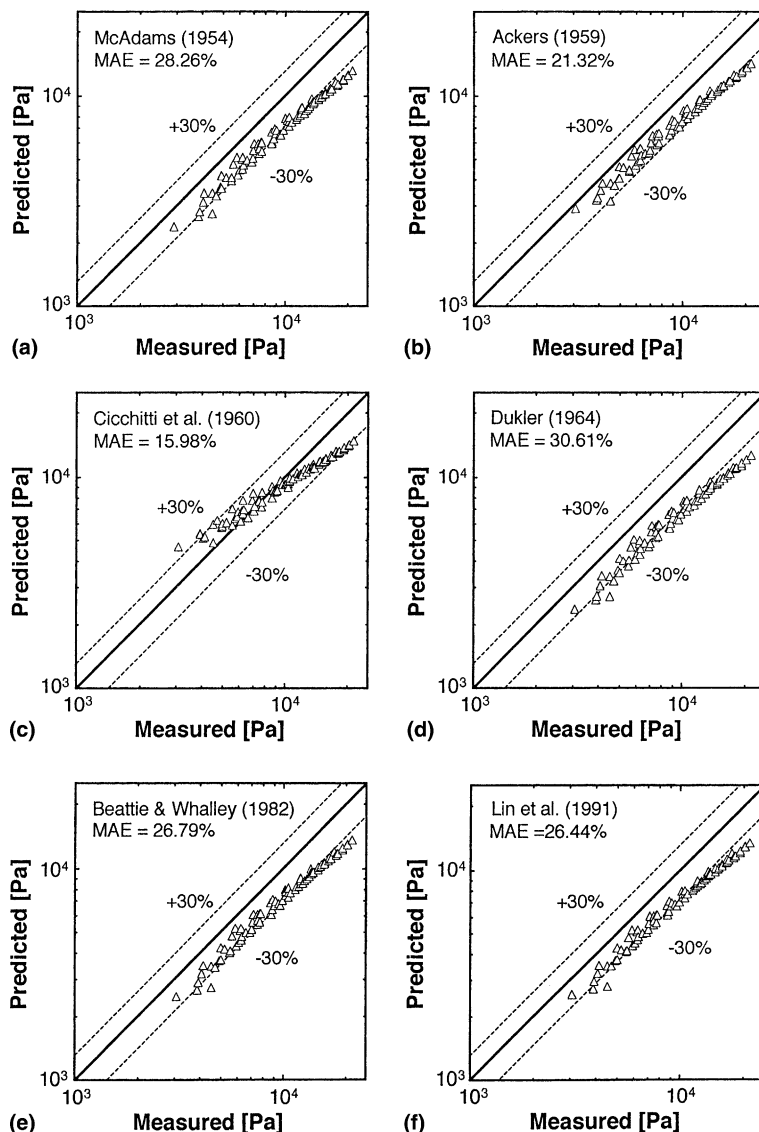


Fig. 3. Comparison of present R134a pressure drop data with homogeneous equilibrium model predictions based on two-phase viscosity models by (a) McAdams [2], (b) Ackers [15], (c) Cicchitti et al. [2], (d) Dukler [2], (e) Beattie and Whalley [16], and (f) Lin et al. [17].

deviation from the data. The trend predicted by the Cicchitti two-phase viscosity model, Fig. 3(c), is somewhat different from that of the other models because this model is quality weighed and therefore provides significantly higher estimates of two-phase mixture viscosity at low quality than the other models. Since the low exit quality data are associated with smaller pressure drop, the Cicchitti model overpredicts these data but underpredicts the high exit quality data. The combination of overprediction at low quality and underprediction at high quality yields a relatively favorable

MAE for the Cicchitti model. Nonetheless, Fig. 3(c) shows this model does not capture the true pressure drop trend.

### 3.2.2. Separated flow model (SFM)

Table 2 summarizes relations that were used to determine the two-phase frictional pressure drop based on the separated flow model, which include two popular macro-channel correlations (Lockhart–Martinelli [1] and Friedel [2]), and three recent small-channel correlations.

Table 2  
Two-phase frictional pressure drop correlations based on separated flow model and corresponding MAE for R134a

Author(s) [Ref.]	Remarks	Frictional pressure drop correlation	MAE (%)
Lockhart and Martinelli [1]	Fluids: water, benzene, kerosene, oil, etc. $d_h = 1.49\text{--}25.83\text{ mm}$	$\Delta P_f = \frac{2G^2 L_{tp}}{d_h x_{e,out}} \int_{x_{e,in}}^{x_{e,out}} f_f(1-x_e)v_f \phi_f^2 dx_e$ $\phi_f^2 = 1 + \frac{C}{X} + \frac{1}{X^2}, X^2 = [(dP/dz)_f / (dP/dz)_g]$ <p><math>C = 5</math> (laminar liquid–laminar vapor), <math>C = 10</math> (turbulent liquid–laminar vapor), <math>C = 12</math> (laminar liquid–turbulent vapor), <math>C = 20</math> (turbulent liquid–turbulent vapor)</p>	14.90
Friedel [2]	$d_h \geq 4\text{ mm}$	$\Delta P_f = \frac{2f_{fo} G^2 L_{tp} v_f}{d_h x_{e,out}} \int_{x_{e,in}}^{x_{e,out}} \phi_{fo}^2 dx_e$ $\phi_{fo}^2 = A_1 + \frac{3.24 A_2 A_3}{Fr_{tp}^{0.045} We_{tp}^{0.035}}$ $A_1 = (1-x)^2 + x^2 \left( \frac{\rho_f f_{go}}{\rho_g f_{fo}} \right), A_2 = x^{0.78} (1-x)^{0.224},$ $A_3 = \left( \frac{\rho_f}{\rho_g} \right)^{0.91} \left( \frac{\mu_g}{\mu_f} \right)^{0.19} \left( 1 - \frac{\mu_g}{\mu_f} \right)^{0.7}$ $Fr_{tp} = \frac{G^2}{gd_h \bar{\rho}^2}, We_{tp} = \frac{G^2 d_h}{\bar{\rho} \sigma}, \bar{\rho} = \frac{1}{x_e v_g + (1-x_e)v_f}$	24.00
Mishima and Hibiki [5]	Fluid: air–water mixture, $d_h = 1\text{--}4\text{ mm}$	$\Delta P_f = \frac{2G^2 L_{tp}}{d_h x_{e,out}} \int_{x_{e,in}}^{x_{e,out}} f_f(1-x_e)v_f \phi_f^2 dx_e$ $\phi_f^2 = 1 + \frac{C}{X} + \frac{1}{X^2}, X^2 = [(dP/dz)_f / (dP/dz)_g]$ $C = 21[1 - \exp(-0.319 \cdot d_h)]; d_h \text{ (mm)}$	34.37
Lee and Lee [8]	Fluid: air–water mixture $d_h = 0.78, 6.67\text{ mm}$	$\Delta P_f = \frac{2G^2 L_{tp}}{d_h x_{e,out}} \int_{x_{e,in}}^{x_{e,out}} f_f(1-x_e)v_f \phi_f^2 dx_e$ $\phi_f^2 = 1 + \frac{C}{X} + \frac{1}{X^2}, X^2 = [(dP/dz)_f / (dP/dz)_g]$ $C = c_1 \lambda^{c_2} \psi^{c_3} Re_{fo}^{c_4}, \lambda = \frac{\mu_f^2}{\rho_f \sigma d_h}, \psi = \frac{\mu_f \dot{J}_f}{\sigma}, c_1, c_2, c_3, c_4$ <p>from Table 4 in Ref. [8]</p>	16.04
Zhang and Webb [9]	Fluids: R134a, R22, R404a, $d_h = 2.13\text{ mm}$	$\Delta P_f = \frac{2f_{fo} G^2 L_{tp} v_f}{d_h x_{e,out}} \int_{x_{e,in}}^{x_{e,out}} \phi_{fo}^2 dx_e$ $\phi_{fo}^2 = (1-x_e)^2 + 2.87x^2 \left( \frac{P}{P_c} \right)^{-1}$ $+ 1.68x_e^{0.8} (1-x_e)^{0.25} \left( \frac{P}{P_c} \right)^{-1.64}$	50.07

The accelerational two-phase pressure drop was expressed in terms of the evaporator’s inlet and outlet conditions [1].

$$\Delta P_a = G^2 \left\{ \left[ \frac{v_g x_{e,out}^2}{\alpha_{out}} + \frac{v_f (1-x_{e,out})^2}{(1-\alpha_{out})} \right] - \left[ \frac{v_g x_{e,in}^2}{\alpha_{in}} + \frac{v_f (1-x_{e,in})^2}{(1-\alpha_{in})} \right] \right\}, \quad (10)$$

where the void fraction was determined from Zivi’s [18] popular relation

$$\alpha = \left[ 1 + \left( \frac{1-x_e}{x_e} \right) \left( \frac{v_f}{v_g} \right)^{2/3} \right]^{-1}. \quad (11)$$

Fig. 4 compares pressure drop predictions of the different separated flow correlations with the experimental data. Interestingly, the predictions of the first two macro-channel correlations are not as poor as first thought. The small-channel correlations show appreciable deviation from the data.

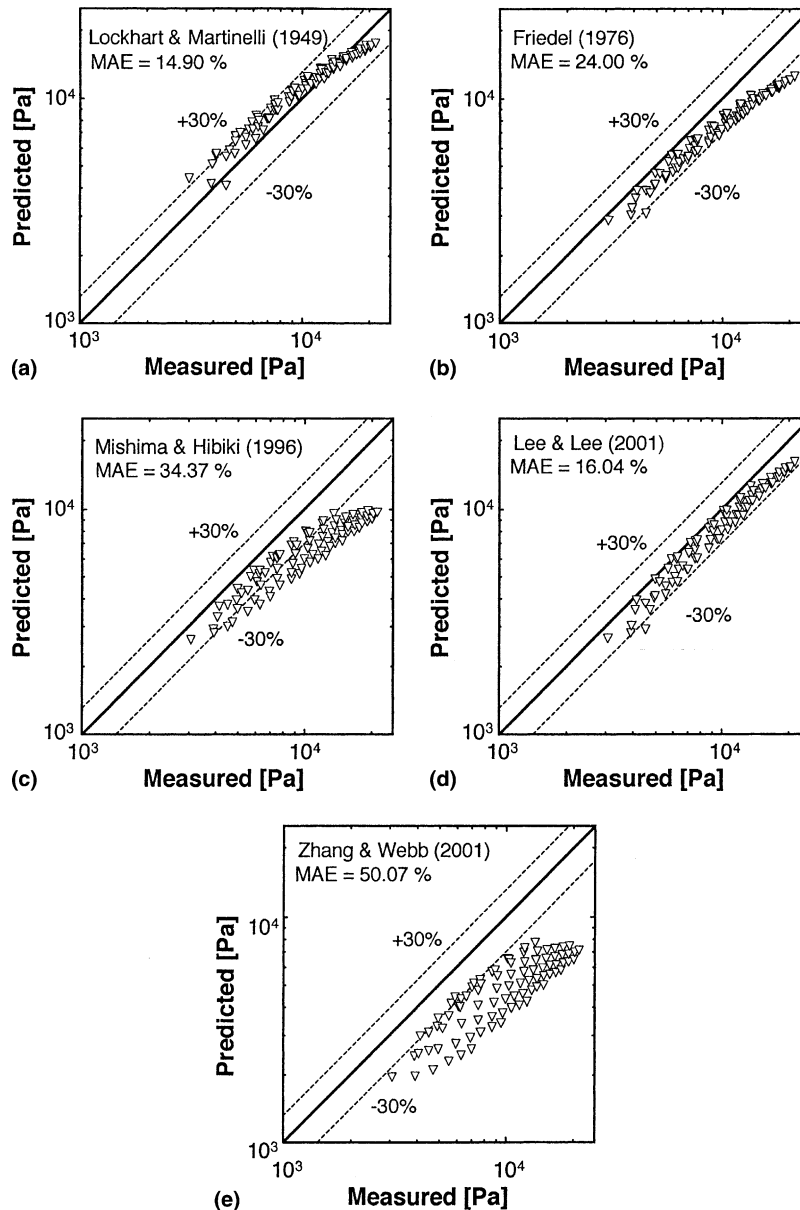


Fig. 4. Comparison of present R134a pressure drop data with separated flow model predictions based on correlations by (a) Lockhart and Martinelli [1], (b) Friedel [2], (c) Mishima and Hibiki [5], (d) Lee and Lee [8], and (e) Zhang and Webb [9].

#### 4. New correlation

A new approach was developed to improve the accuracy of pressure drop prediction in two-phase micro-channels. Since the bubbly and churn flow patterns are rarely detected in high-flux micro-channel flow [10,12], the separated flow model was deemed more appropriate than the homogeneous. This is especially the case with the present R134a experiments where the fluid entered the micro-channels as a two-phase mix-

ture. Video imaging in the present study proved the flow was predominantly slug or annular, especially at high-heat fluxes.

In both the slug and annular regimes, mass transfer by liquid breakup and deposition is highly influenced by surface tension. A new parameter is therefore sought to incorporate this effect in the separated flow model. Lee and Lee [8] used the same rationale and suggested incorporating several dimensionless groups (see Table 2) in the two-phase multi-

plier relation. As shown in Fig. 4(d), their approach showed more favorable predictions of the present R134a data than the other two small-channel correlations.

A more mechanistic approach is adopted in the present study. It is assumed the added complexity of two-phase flow in a micro-channel is the net result of interactions between liquid inertia, liquid viscous force, and surface tension. Two key measures of these interactions are the Reynolds and Weber numbers based on liquid properties.

$$Re_{fo} = \frac{Gd_h}{\mu_f} \tag{12a}$$

and

$$We_{fo} = \frac{v_f G^2 d_h}{\sigma} \tag{12b}$$

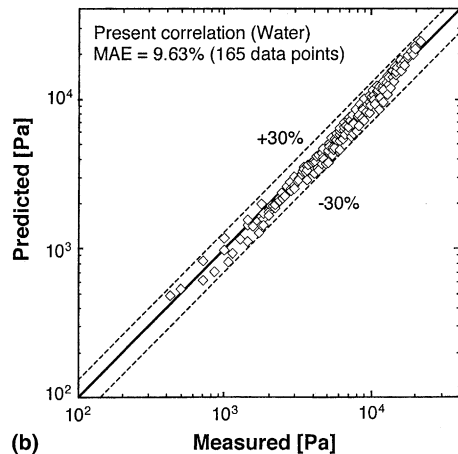
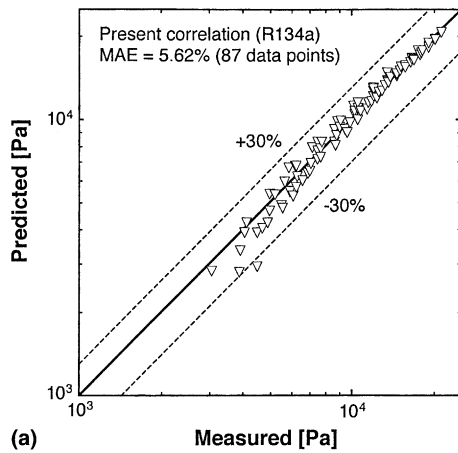


Fig. 5. Comparison of new correlation predictions with (a) present R134a data and (b) Qu and Mudawar’s [12] micro-channel water data.

The two-phase pressure drop multiplier

$$\phi_r^2 = 1 + \frac{C}{X} + \frac{1}{X^2} \tag{13}$$

is modified with a new dimensionless parameter defined as

$$C = c_1 Re_{fo}^{c_2} We_{fo}^{c_3} \tag{14}$$

To enhance the predictive capability of the new correlation, both the present R134a data and prior micro-channel water data of Qu and Mudawar [12] were examined. Large differences between the thermophysical properties of the two coolants were deemed highly effective at broadening the application range of the new correlation. Another key difference between the two data sets is both the liquid and vapor flows are laminar for the water data, while low viscosity rendered the vapor flow turbulent for R134a. Typical micro-channel

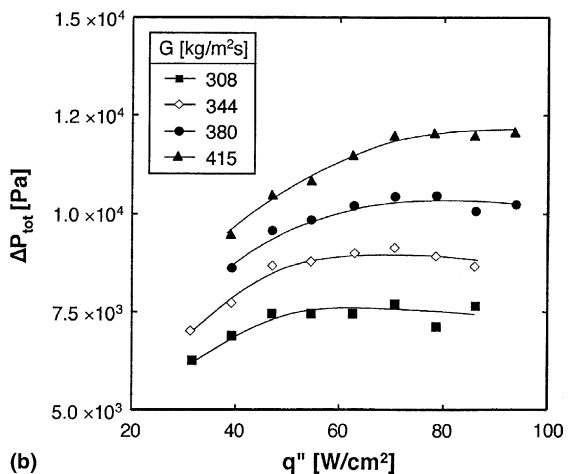
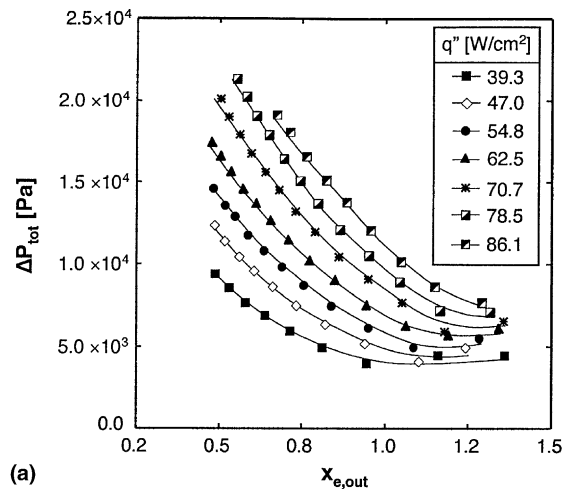


Fig. 6. Variation of measured R134a total pressure drop with (a) exit quality for different heat fluxes, and (b) heat flux for different mass velocities.

operating conditions rarely produce turbulent liquid flow. Therefore, two separate correlations were derived for  $C$  based on the flow states of the liquid and vapor,

$$C_{vv} = 2.16Re_{fo}^{0.047} We_{fo}^{0.60} \quad (\text{laminar liquid–laminar vapor}) \quad (15a)$$

$$C_{vt} = 1.45Re_{fo}^{0.25} We_{fo}^{0.23} \quad (\text{laminar liquid–turbulent vapor}) \quad (15b)$$

Notice the stronger effect of surface tension where both liquid and vapor are laminar.

Fig. 5(a) shows excellent agreement of the pressure drop predictions based on the new correlation with the R134a data, both in terms of MAE and general trend. The largest deviation is concentrated in the low mass flux and low heat flux region where both the heat loss (which influences the accuracy of the heat flux used in the pressure drop model) and the flow rate measurement uncertainty are greatest.

Fig. 5(b) shows the present correlation is also very effective at predicting the micro-channel water data of Qu and Mudawar [12].

### 5. Dominant features of two-phase pressure drop

The newly developed correlation was used to explore several important trends concerning pressure drop in the present R134a study. Fig. 6(a) shows, for a constant heat flux, the two-phase pressure drop decreases with increasing outlet quality due mostly to decreasing mass velocity. This decrease appears to subside around an exit quality value of unity. Fig. 6(b) shows increasing heat flux for a constant mass velocity increases pressure drop up to a particular heat flux value beyond which pressure drop becomes constant or slightly decreases.

These trends can be explained by exploring the variations of individual components of pressure drop. Fig. 7 shows the contributions of these components to total pressure drop. For a constant mass velocity, the two-phase frictional and accelerational losses both increase with increasing heat flux up to a particular heat flux value corresponding to complete conversion into vapor. Beyond this point, the two-phase frictional loss decreases as the two-phase region begins to occupy a smaller portion of the channel length. However, the accelerational loss becomes constant beyond

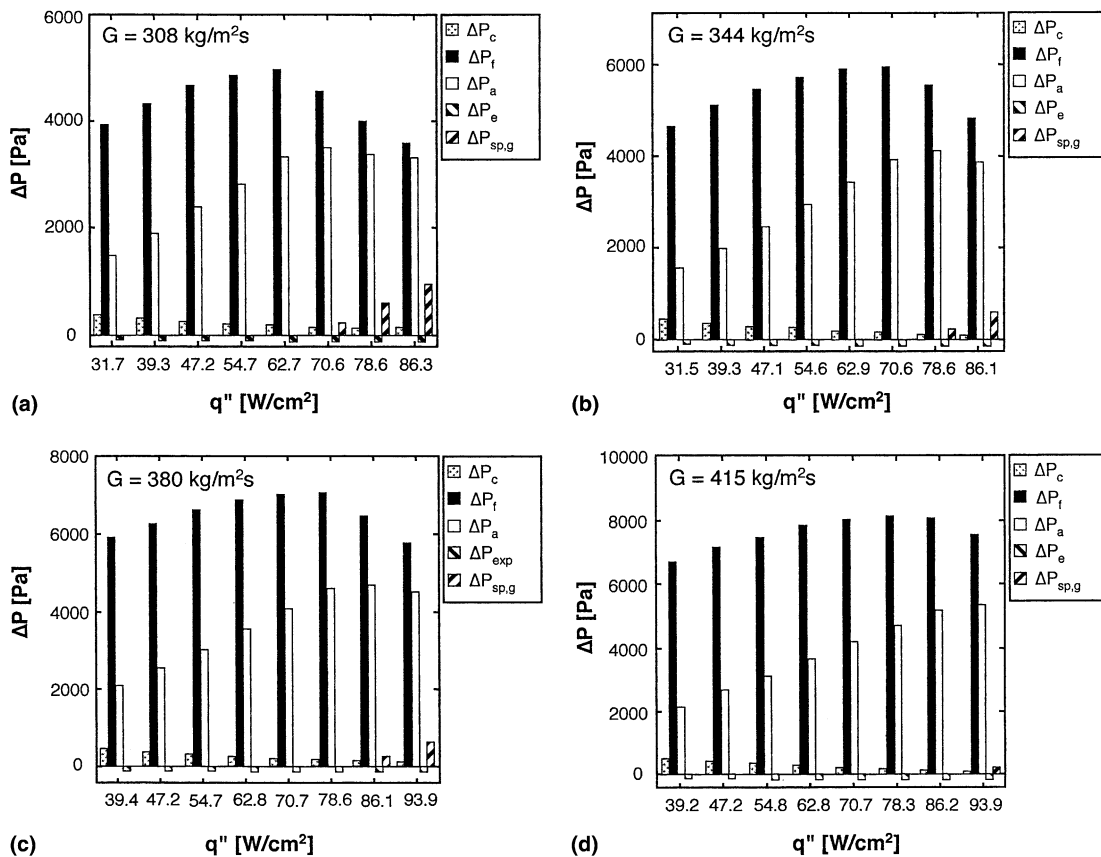


Fig. 7. Individual components of pressure drop for different heat fluxes and mass velocities of (a) 308, (b) 344, (c) 380, and (d) 415  $kg/m^2s$ .

the same point as the flow is converted completely into vapor. Since the downstream portion of the channel is now occupied mostly by vapor, the decreased two-phase frictional loss is compensated for by a measurable increase in the single-phase vapor pressure loss. This explains why the total pressure drop becomes constant or decreases slightly with increasing heat flux beyond the point of full conversion into vapor.

**6. Flow instabilities**

Intrinsic to any refrigeration cycle, the throttling valve located upstream of the evaporator offers important benefits to the operation of a micro-channel evaporator. Qu and Mudawar [12] proved the interaction of the two-phase mixture with the upstream compressible volume in a flow loop can trigger ‘severe pressure oscillation’ which is also a precursor for premature critical heat flux (CHF). The throttling valve in the present system imparted greater stiffness to the system, precluding both this severe form of instability and the premature CHF.

Despite its effectiveness at suppressing the severe pressure oscillation, the micro-channel evaporator is still susceptible to a second ‘parallel channel instability’

[12] caused by interaction between micro-channels within the heat sink itself. This instability is quite random in nature and much milder than the aforementioned ‘severe pressure oscillation.’ This is demonstrated in Fig. 8 in the form of temporal variations of pressure drop for different mass velocities at four representative heat fluxes. It is important to point out that mass velocity is strongly tied to the amount of throttling upstream of the evaporator. Reducing the throttling increases the mass velocity but increases the parallel channel instability as well. This trend is clearly evident in Fig. 8(b) and (c). Despite the seemingly large increase in instability, the reader is cautioned that the amplitude of pressure fluctuation at the highest mass velocity of  $G = 621 \text{ kg/m}^2 \text{ s}$  is only about 4000 Pa, which is hardly a reason for concern in a practical refrigeration system.

Fig. 8 provides valuable insight into the effect of heat flux on flow instability. Comparing Fig. 8(c) and (d) shows increasing the heat flux for the same mass velocity aids in stabilizing the flow. This is apparently due to the higher heat flux increasing vapor production causing (1) a smaller portion of the micro-channel length being occupied by the two-phase mixture and (2) increasing pressure drop. Both effects increase the evaporator’s stiffness for a given amount of upstream throttling.

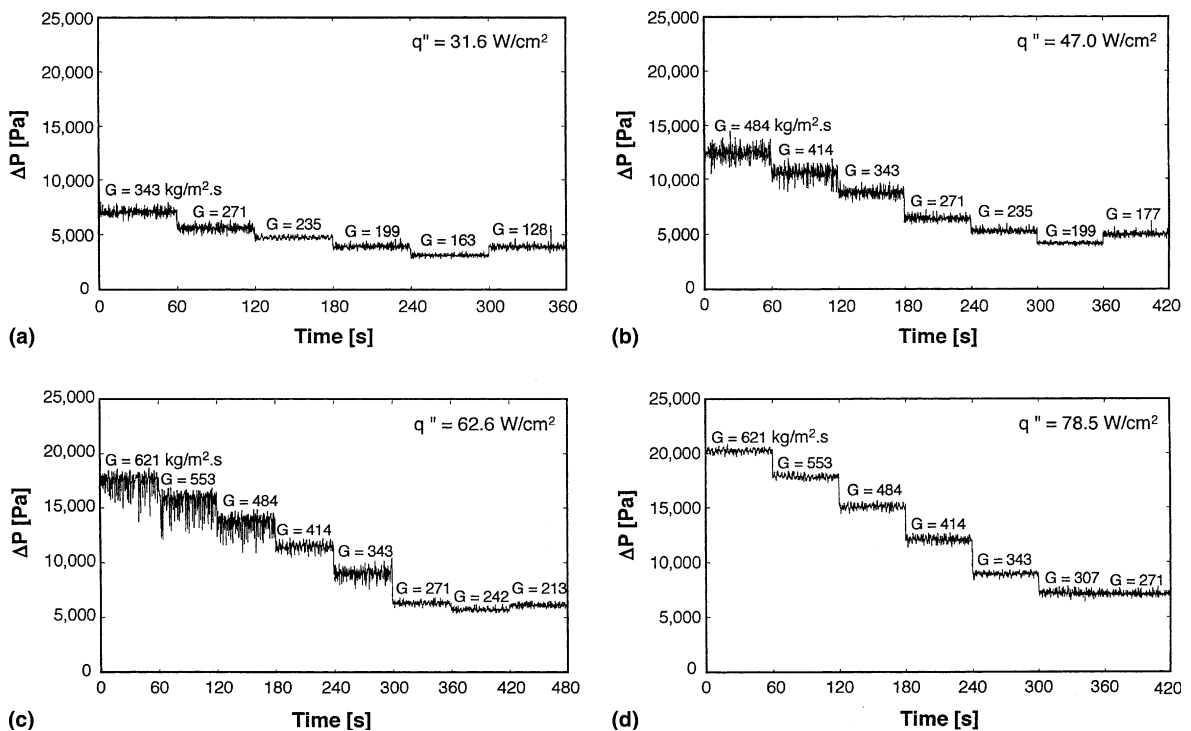


Fig. 8. Temporal variations of pressure drop for heat fluxes of (a) 31.6, (b) 47.0, (c) 62.6, and (d) 78.5  $\text{W/cm}^2$ .

## 7. Conclusions

The pressure drop characteristics were investigated experimentally for a heat sink with parallel rectangular micro-channels that served as an evaporator in an R134a refrigeration cycle. Both homogeneous equilibrium and separated flow models were assessed for accuracy in predicting the new data, and a new correlation was developed to improve the overall predictive capability of the latter. Key findings from the study are as follows:

- (1) Using several popular two-phase viscosity models, the homogeneous equilibrium model generally underpredicted the present R134a data.
- (2) Popular macro-channel separated flow model correlations generally yielded better predictions of pressure drop than some recent small-channel correlations.
- (3) Since two-phase flow in high-flux micro-channel heat sinks is predominantly slug or annular, a new correlation was developed that was based on the separated flow model. The new correlation incorporates the effects of liquid inertia, viscous force and surface tension on the two-phase pressure drop multiplier. Excellent agreement is achieved between pressure drop predictions based on the new correlation and both present R134a data and prior micro-channel water data.
- (4) The total pressure drop generally increases with increasing mass velocity and/or heat flux. However, there is appreciable diminution in this increase where complete conversion to vapor takes place inside the micro-channels.
- (5) The throttling valve in a refrigeration cycle offers important benefits to the operation of a micro-channel evaporator. By stiffening the system against interactions between the two-phase flow in the evaporator and the upstream compressible volume, the throttling valve serves to suppress any large pressure oscillations, allowing only mild parallel channel instability to take place.

## Acknowledgment

The authors are grateful for the support of the Office of Naval Research (ONR) for this research.

## References

- [1] R.W. Lockhart, R.C. Martinelli, Proposed correlation of data for isothermal two-phase, two-component flow in pipes, *Chem. Eng. Prog.* 45 (1949) 39–48.
- [2] J.G. Collier, J.R. Thome, *Convective Boiling and Condensation*, third ed., Oxford University Press, Oxford, 1994.
- [3] D. Chisholm, Pressure gradients due to friction during the flow of evaporation two-phase mixtures in smooth tubes and channels, *Int. J. Heat Mass Transfer* 16 (1973) 347–358.
- [4] M.B. Bowers, I. Mudawar, Two-phase electronic cooling using mini-channel and micro-channel heat sinks. Part 2: flow rate and pressure drop constraints, *ASME J. Electron. Packag.* 116 (1994) 298–305.
- [5] K. Mishima, T. Hibiki, Some characteristics of air–water two-phase flow in small diameter vertical tubes, *Int. J. Multiphase Flow* 22 (1996) 703–712.
- [6] K.A. Triplett, S.M. Ghiaasiaan, S.I. Abdel-Khalik, A. LeMouel, B.N. McCord, Gas–liquid two-phase flow in microchannels. Part II: void fraction and pressure drop, *Int. J. Multiphase Flow* 25 (1999) 395–410.
- [7] T.N. Tran, M.-C. Chyu, M.W. Wambsganss, D.M. France, Two-phase pressure drop of refrigerants during flow boiling in small channels: an experimental investigation and correlation development, *Int. J. Multiphase Flow* 26 (2000) 1739–1754.
- [8] H.J. Lee, S.Y. Lee, Pressure drop correlations for two-phase flow within horizontal rectangular channels with small heights, *Int. J. Multiphase Flow* 27 (2001) 783–796.
- [9] M. Zhang, R.L. Webb, Correlation of two-phase friction for refrigerants in small-diameter tubes, *Exp. Therm. Fluid Sci.* 25 (2001) 131–139.
- [10] A. Kawahara, P.M.-Y. Chung, M. Kawaji, Investigation of two-phase flow pattern void, fraction and pressure drop in a microchannel, *Int. J. Multiphase Flow* 28 (2002) 1411–1435.
- [11] W. Qu, I. Mudawar, Experimental and numerical study of pressure drop and heat transfer in a single-phase micro-channel heat sink, *Int. J. Heat Mass Transfer* 45 (2002) 2549–2565.
- [12] W. Qu, I. Mudawar, Measurement and prediction of pressure drop in two-phase micro-channel heat sinks, *Int. J. Heat Mass Transfer* 46 (2003) 2737–2753.
- [13] R.K. Shah, A.L. London, *Laminar Flow Forced Convection in Ducts: A Source Book of Compact Heat Exchanger Analytical Data*, Academic Press, New York, 1978 (Suppl. 1).
- [14] F.P. Incropera, D.P. Dewitt, *Fundamentals of Heat and Mass Transfer*, fifth ed., Wiley, New York, 2002.
- [15] Y.-Y. Yan, T.-F. Lin, Evaporation heat transfer and pressure drop of refrigerant R-134a in a small pipe, *Int. J. Heat Mass Transfer* 41 (1998) 4183–4194.
- [16] D.R.H. Beattie, P.B. Whalley, A simple two-phase flow frictional pressure drop calculation method, *Int. J. Multiphase Flow* 8 (1982) 83–87.
- [17] S. Lin, C.C.K. Kwok, R.Y. Li, Z.H. Chen, Z.Y. Chen, Local frictional pressure drop during vaporization for R-12 through capillary tubes, *Int. J. Multiphase Flow* 17 (1991) 95–102.
- [18] S.M. Zivi, Estimation of steady-state stem void-fraction by means of the principle of minimum entropy production, *ASME J. Heat Transfer* 86 (1964) 247–252.